

## PERFORMANCE OF THE LOW-REYNOLDS $\kappa$ - $\epsilon$ LSH MODEL TO PREDICT FLOW THROUGH CURVILINEAR OBSTRUCTION

G. N. Zevallos – gzevallo@mec.puc-rio.br

A. O. Nieckele – nieckele@mec.puc-rio.br

Departamento de Engenharia Mecânica, Pontifícia Universidade Católica – PUC/Rio  
R. Marquês de São Vicente 225- Gávea, 22453-900 Rio de Janeiro, RJ, Brasil

**Abstract.** *Turbulent flows inside curvilinear obstruction tubes are encountered in many engineering situations. The prediction of flows in the presence of separation and reattachment is a difficult task. Several low-Reynolds number turbulence models have been developed aiming a better prediction of the recirculation areas, as well as pressure recovery after the obstruction and shear stress distribution along the duct walls. At the present work, the curvilinear obstruction is described by a cosine curve. For this geometry, the  $\kappa$ - $\epsilon$  low Reynolds number turbulence model LSH presents a reasonable prediction for the mean flow field and pressure drop, however it fails to predict the turbulent quantities. The objective of the present paper is to analyze the influence of different low-Reynolds correction terms in the LSH model. Therefore, a few modifications were introduced in the original model. The velocity, turbulent kinetic energy and dissipation rate fields obtained by the different model modifications are compared with numeric and experimental data found in the literature. The numeric determination of the fluid flows was accomplished by a finite volume method. Among all model modifications that have been tested, none was able to reproduce exactly the experimental data.*

**Key-words:** *Low Reynolds  $\kappa$ - $\epsilon$  models, curvilinear obstruction*

### 1. INTRODUCTION

Numerical simulation of flow field has become an excellent tool to help develop projects and process that are more efficient at a lower cost. For engineering applications, in general the flow field is turbulent. Since turbulent flow is three dimensional and transient, the computing effort to obtain directly the velocity and pressure field, especially in complex geometries, is very high. An attractive alternative from the practical point of view is to employ turbulence models to predict the time average variables of interest. Among the two equation differential models available, the high Reynolds numbers  $\kappa$ - $\epsilon$  model is still the model more widely used to solve practical engineering problems. The traditional  $\kappa$ - $\epsilon$  model has been significantly enhanced to be applied to the whole domain, i.e, in the near wall region as well as in the turbulent core. These models are called low Reynolds number  $\kappa$ - $\epsilon$  models (LRN), since they can predict the flow behavior near the walls, where the local Reynolds number is low. They are obtained by the introduction of some correction terms for the wall region in the traditional  $\kappa$ - $\epsilon$  model. Along the last decades, several works have been published, with different

variants of the model. Just a few of them are referred here: Jones and Launder, 1972, Patel and Rodi, (1985), Koobus (1994), Geronimos and So (1997) and Chen et al. (1998).

Flow field in curvilinear obstructions is often found in engineering applications. An example that can be mentioned is the presence of weld joints in small diameter ducts which causes localized corrosion after the restriction. The prediction of the pressure recovery and the shear distribution along the obstruction can help to design equipment to avoid the corrosion (Rastogi, 1984). Zevallos and Nieckele (1999) investigated the performance of three different low Reynolds number models to predict the flow field in a duct with a curvilinear obstruction defined by a cosine curve. The model developed by Hanjalic and Launder (1980) presented the best prediction of the mean flow field and pressure distribution, however no model was able to reproduce the turbulent quantities.

The main objective of the present work is to analyze the influence, in the numerical solution of the flow field, of the different correction terms of the Hanjalic and Launder (1980) model. In addition, verify whether modifications in the selected model are capable of better capturing the recirculation areas and pressure recovery after the obstruction, which are fundamental in the evaluation of the shear distribution.

## 2. ANALYSIS

The geometry selected to be analyzed at the present work consists of a duct with circular cross-section, with a curvilinear obstruction as illustrated in Fig. 1. The obstruction is defined by a stenosis type of curve, described by the following expression

$$R_c / R_o = 1 - \delta / 2R_o [1 + \cos (\pi x / x_o)] \quad (1)$$

where  $R_c$  is the duct radius,  $R_o$  the unobstructed duct radius,  $\delta$  is restriction height,  $x$  is the axial coordinate and  $x_o$  is the restriction half length. The dimensionless parameters that characterized the obstruction were set as  $x_o/R_o = 2$  and  $\delta/R_o = 0.5$ . The length of the straight duct upstream and downstream the obstruction

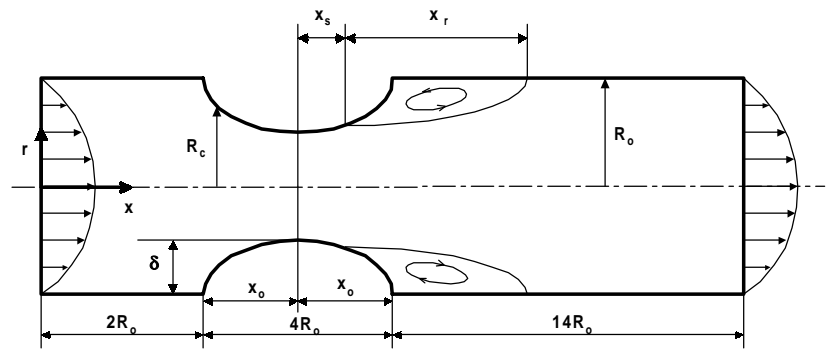


Figure 1- Duct with curvilinear obstruction.

were set at  $x_{up}/R_o = 2$ , and  $x_{dn}/R_o = 14$ . This configuration was experimentally investigated by Deshpande e Giddens, 1980. Numerical investigation based on the standard  $\kappa$ - $\epsilon$  model has also been performed for this configuration by Rastogi (1984), Melaaen (1992) e Zijlema et al. (1995).

To obtain the flow field in a horizontal axi-symmetric duct, the following hypotheses were made: Newtonian fluid, constant properties and steady state regime. The average continuity and momentum equations, based on the Boussinesq approximation, can be written as:

$$\frac{\partial u_i}{\partial x_i} = 0 \quad (2)$$

$$\rho u_j \frac{\partial u_i}{\partial x_j} = \frac{\partial}{\partial x_j} \left[ (\mu + \mu_t) \left( \frac{\partial u_i}{\partial x_j} + \frac{\partial u_j}{\partial x_i} \right) \right] - \frac{\partial P}{\partial x_i} \quad (3)$$

where  $u_j$  are the velocity components,  $x_j$  the coordinate directions,  $\mu$  and  $\mu_t$  are the absolute and turbulent viscosity,  $\rho$  is the density and  $P$  is a modified pressure [ $P = p + (2/3) \rho \kappa$ ], where  $\kappa$  is the turbulent kinetic energy.

Zevallos and Nieckele (1999) investigated the performance of different low Reynolds number models to predict the flow field in the present configuration. Based on their analysis, the model developed by Launder and Sharma and modified by Hanjalic, (Hanjalic and Launder, 1980) was selected to be further examined, due to its ability to represent the flow near the wall. This model will be referred here as the LSH model. For the LSH model, the turbulent viscosity  $\mu_t$  is

$$\mu_t = f_\mu c_\mu \rho \kappa^2 / \tilde{\epsilon} \quad (4)$$

where  $f_\mu$  is a damping function, defined as

$$f_\mu = \exp \left[ -3.4 / (1 + 0.02 Re_t^2) \right] \quad (5)$$

which depends on the local Reynolds number  $Re_t$ , given by

$$Re_t = \rho \kappa^2 / (\mu \tilde{\epsilon}) \quad (6)$$

$c_\mu = 0.09$  is an empirical constant and  $\tilde{\epsilon}$  is a pseudo dissipation rate of the turbulent kinetic energy  $\kappa$ , defined as

$$\tilde{\epsilon} = \epsilon - \epsilon_w \quad ; \quad \epsilon_w = 2\mu \left( \frac{\partial \sqrt{\kappa}}{\partial x_j} \right) \left( \frac{\partial \sqrt{\kappa}}{\partial x_j} \right) \quad (7)$$

where  $\epsilon$  is the dissipation rate of the turbulent kinetic energy  $\kappa$ . This variable is introduced to simplify the definition of the boundary condition for the dissipation equation, which becomes zero.

The turbulent kinetic energy  $\kappa$  conservation equation for the LSH model can be represented by the following equation,

$$\rho u_j \frac{\partial \kappa}{\partial x_j} = \frac{\partial}{\partial x_j} \left[ \left( \mu + \frac{\mu_t}{\sigma_\kappa} \right) \frac{\partial \kappa}{\partial x_j} \right] + P_\kappa - \rho \tilde{\epsilon} + L_\kappa \quad (8)$$

where  $\sigma_\kappa = 1.0$  is an empirical constant, and  $P_\kappa$  is the production of turbulent kinetic energy, given by

$$P_\kappa = \mu_t \left[ \frac{\partial u_i}{\partial x_j} + \frac{\partial u_j}{\partial x_i} \right] \frac{\partial u_i}{\partial x_j} \quad (9)$$

$L_\kappa$  is the term extra of the turbulent kinetic energy equation, due to the adoption of the pseudo dissipation rate

$$L_\kappa = \rho \epsilon_w \quad (10)$$

The pseudo dissipation rate of the turbulent kinetic energy  $\tilde{\epsilon}$  conservation equation is

$$\rho u_j \frac{\partial \tilde{\varepsilon}}{\partial x_j} = \frac{\partial}{\partial x_j} \left[ \left( \mu + \frac{\mu_t}{\sigma_\varepsilon} \right) \frac{\partial \tilde{\varepsilon}}{\partial x_j} \right] + P_\varepsilon - C_2 f_2 \rho \frac{\tilde{\varepsilon}^2}{\kappa} + L_\varepsilon \quad (11)$$

where  $\sigma_\varepsilon = 1.30$  and  $C_2 = 1.92$  are empirical constants.  $P_\varepsilon = C_1 \varepsilon / \kappa P_\kappa$  is the production of dissipation of turbulent kinetic energy. It represents the generation of vorticity due to vortices stretching induced by turbulence. Hanjalic (1980) suggests that this term must be modified to take in account in transfer of kinetic energy not only due to the rotational part of the stress, but the irrotational part as well. The generation of dissipation should be governed by the normal stress. Therefore,  $P_\varepsilon$  was divided in two parts in order to give different weights to the normal and tangential stress contribution to  $P_\varepsilon$ , which is then given by

$$P_\varepsilon = [C_1 P_\kappa (1 - \delta_{ij}) + C_3 P_\kappa \delta_{ij}] (\tilde{\varepsilon} / \kappa) \quad (12)$$

where  $C_1 = 1.44$  and  $C_3 = 4.44$  are empirical constants. In the above equation,  $P_\kappa \delta_{ij}$  implies the normal stress contribution and  $P_\kappa (1 - \delta_{ij})$  the tangential stress contribution.

The correction terms introduced in the traditional  $\kappa$ - $\varepsilon$  model to represent the flow near the walls are the damping functions  $f_\mu$  and  $f_2$  and the additional source terms  $L_\varepsilon$  in  $\tilde{\varepsilon}$  conservation equation. The damping function  $f_2$  is

$$f_2 = 1 - 0.3 \exp(-Re_t^2) \quad (13)$$

The  $L_\varepsilon$  term is introduced in the original LSH model, to better represent a peak of kinetic energy observed in experimental data for the jet flow, and it is given as

$$L_\varepsilon = \frac{2\mu \mu_t}{\rho} \left[ \frac{\partial}{\partial x_j} \left( \frac{\partial u_i}{\partial x_k} \right) \right]^2 \quad (14)$$

The modifications implemented in the LSH model have been made with the objective of investigating of the influence of extra term  $L_\varepsilon$  and the production term coefficients  $C_1$  and  $C_3$  in the dissipation equation. These terms have been empirically introduced in the dissipation equation. Logically, in order to evaluate the results of the modifications, only one term is modified at a time while every other term is kept equal to the one in the original model.

The first modification introduced was to equate the generation term constants  $C_1$  and  $C_3$  in the dissipation rate equation. This has been done in order to provide the same weighting factor to the normal and shear stresses and to verify whether different weighting factors have a great influence in the turbulent kinetic energy dissipation rate. This case is named as  $C_3 = C_1$ .

The second modification introduced was the omission of the extra term in the dissipation rate equation as this term had been introduced in the LSH model, without any good explanation, for a jet flow. The results due to this modification are referred here as  $L_\varepsilon = 0$ ,  $C_3 \approx 3C_1$ .

The third modification performed consisted of not only omitting the extra term in the dissipation rate equation, but also equating the constants of the generation term of the dissipation term. The objective is to verify whether the combined effects could lead to improvements in the obtained results. This case is referred as  $L_\varepsilon = 0$ ,  $C_3 = C_1$ .

The last modification was to investigate, in the absence of  $L_\varepsilon$ , another combination of the weights given to the normal and tangential stress contribution to the production of  $\varepsilon$ . The strength of the normal stress contribution was reduced and defined as only twice the strength of the tangential contribution. Thus, this case is referred as  $L_\varepsilon = 0$ ,  $C_3 = 2C_1$ .

## 2.1 Boundary conditions

At the inlet, a fully developed velocity profile,  $u_{in}$ , was specified in accordance with the experimental data of Deshpande and Giddens 1980, as

$$u_{in} = 1.25 u_m \left( 1 - r / R_o \right)^{1/6.4} \quad (15)$$

where  $u_m$  is the mean velocity at the cross section. The boundary conditions, for the turbulent quantities  $\kappa$  and  $\varepsilon$ , were not specified in the experimental work. The turbulent kinetic energy  $\kappa$  was specified as,  $\kappa_{in} = 1.5 (I_{it} u_m)^2 / 2$  where  $I_{it}$  is the turbulence intensity, defined as 3% in accordance with the numerical simulation of this case by Melaaen (1992) and Zijlema et al, (1995). For the dissipation rate, based on the recommendation of Shinha and Candler, (1998), the following expression was adopted,  $\varepsilon_{in} = c_\mu^{3/4} \kappa_{in}^{3/2} / (4 \ell_{in})$ , where  $\ell_{in}$  is the mixing length, and it was defined as  $\ell_{in} = \min[ K (R_o - r); 0.1 R_o ]$  where  $K=0.4$  is the von Kármán constant.

At the symmetry line, the normal velocity component was set equal to zero as well as the normal gradient of all others variables. At the exit plane, the traditional boundary condition of neglecting the diffusion flux of all variables was employed. At the solid surfaces, the non-slip condition was enforced.

## 3. NUMERICAL METHOD

A non-orthogonal curvilinear system of coordinates, which adapts to the boundaries of the domain, was employed. This is an important technique, which allows an easy and exact representation of the boundary conditions, making it possible to solve turbulent flow field in complex geometries. The conservation equations are discretized with the aid of the finite volume method described in Patankar (1980), using the *power-law* scheme. Staggered velocity components were used to avoid unrealistic pressure fields, and the contra-variant velocity component was selected as the dependent variable in the momentum conservation equations (Pires and Nieckele, 1994). The pressure-velocity coupling was solved by an algorithm based on SIMPLEC (van Doormaal and Raithby, 1984). The resulting algebraic system was solved via the TDMA line-by-line algorithm (Patankar, 1980) with the block correction algorithm (Settari and Aziz, 1973) to increase the convergence rate.

To define the mesh size a grid test was performed, where different mesh sizes and distribution were investigated. Finally, a non-uniform 115 x 60 points mesh was specified to analyze the numerical prediction of the flow field. The grid points were concentrated near the solid wall and the obstruction region. The commercial software FLUENT (FLUENT, Inc.V 4.4, 1996) generated the mesh, which is illustrated in Figure 2. The dimensionless wall distance is often used to guide the grid distribution. It is defined as  $y^+ = \rho u^* n / \mu$  where  $n$  is the distance to the wall of the first node point and  $u^* = \sqrt{\tau_w / \rho}$  is the friction velocity where  $\tau_w$  is the wall shear stress. Since at the separation point,  $y^+ = 0$ , this variable is not employed in the LSH model. For the mesh distribution employed in this work, approximately 3 points were specified for the region where  $y^+ < 15$ .

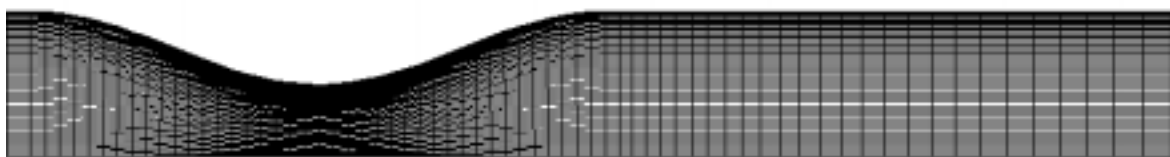


Figure 2 – Non uniform mesh with 115 x 60 grid points.

## 4. RESULTS

The present problem is governed by the several geometric parameters presented and by the Reynolds number defined as  $Re = \rho u_m 2 R_o / \mu$ . For the present work, the Reynolds number was set equal to 15 000.

To evaluate the effect of the modifications in the selected model, the velocity, pressure and turbulence quantity fields were compared with experimental data of Desphande and Giddens (1980), and the numerical results Melaaen (1992), based on the traditional  $\kappa$ - $\epsilon$  model.

Melaaen (1992) solution was obtained with a non-orthogonal coordinate system, with collocated cartesian velocity as the dependent variable, with a mesh size of 52 x 22 nodal points. Melaaen (1992) investigated two interpolation schemes. The first one, based on the power-law scheme, is not presented here. The second case, selected to be compared here, employed a second order upwind interpolation scheme for the velocities and the power-law scheme for the turbulent quantities. The same geometry was also investigated with the traditional  $\kappa$ - $\epsilon$  model by Rastogi (1984) and Zijlema et al, (1995).

### 4.1 Pressure and velocity distribution

To analyze the pressure prediction along the wall, a pressure coefficient was defined based on the inlet pressure  $p_{in}$  and mean velocity  $u_m$  as

$$C_p = (p - p_{in}) / \rho u_m^2 \quad (16)$$

The pressure distribution along the pipe wall is presented at Fig. 3. The dimensionless centerline velocity  $U_c = u_c / u_m$  along the axial direction is presented at Fig. 4. It can be seen that all modifications in the selected model presented a similar behavior in the upstream and convergent section of the duct, both for pressure along the wall and centerline axial velocity.. The results of all models super-estimate the minimum pressure, which occurs at the center of the obstruction ( $x/R_o = 4$ ) and under estimate the maximum velocity. At the divergent section and at the downstream portion of the duct through the exit ( $4 < x/R_o < 20$ ), only the original LHS model is able to satisfactory reproduce the smooth pressure recovery, presenting good agreement with experimental data. Although the LSH underestimates the maximum velocity, it is capable of capturing the flow desacceleration at the divergent region, up to the section  $x/R_o = 6$ , since an excellent agreement with the experimental data is observed. After the end of the obstruction,  $x/R_o = 8$ , it can be seen from the experimental data, a fast velocity recovery to its initial value at  $x/R_o = 14$ . The LSH model does not predict this desacceleration. It is only

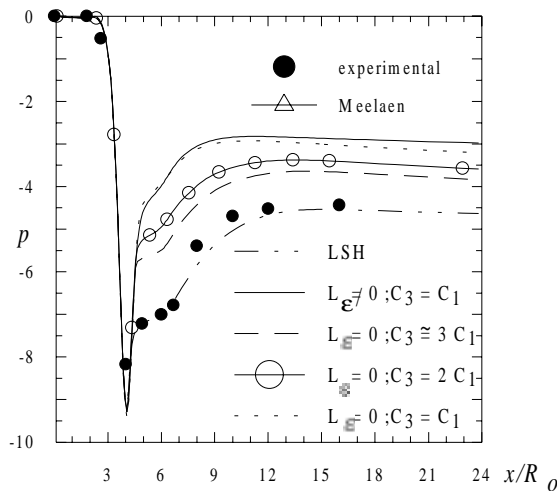


Figure 3 – Pressure coefficient

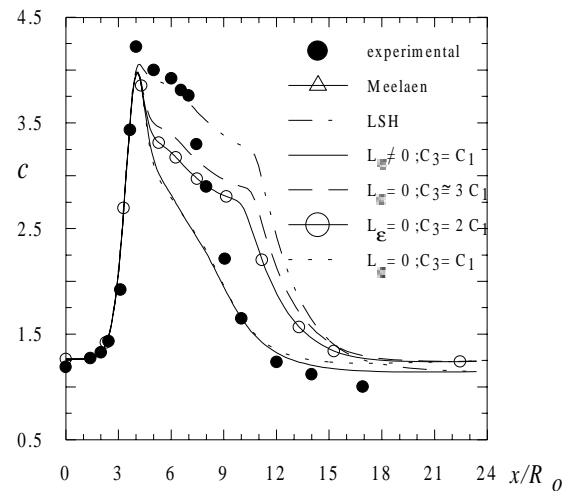


Figure 4 – Centerline velocity distribution

at  $x/R_o = 10.5$  that a strong desacceleration is observed.

Analyzing the pressure distribution and velocity distribution, one can conclude that in fact the normal stress does have a strong influence in the production of  $\varepsilon$ . When both stresses have the same influence, the pressure recovery is super-estimated, resulting in a strong velocity desacceleration beginning at the center of the obstruction. The effect of the extra source term in the  $\varepsilon$  equation is not as significant as the normal stress contribution. When the two constants are the same ( $C_1 = C_3$ ), the presence of  $L_\varepsilon$  in the equation  $\varepsilon$  is not even felt. When  $L_\varepsilon = 0$ , the pressure and velocity distribution obtained are similar to the original LSH, however the pressure after the obstruction is still higher than the experimental data and the velocity recovery is anticipated. Note that the results obtained when  $L_\varepsilon = 0$  is very similar to the results obtained, with higher order interpolation scheme of Melaen (1992), with the traditional  $\kappa$ - $\varepsilon$  model. Note that for  $L_\varepsilon = 0$ , as the weight of the normal stress increases, the pressure and velocity distributions get closer to the experimental data.

## 4.2 Friction factor and reattachment point

The friction factor, or dimensionless wall shear stress,  $\tau_s$ , can be defined as

$$C_f = \tau_s / (0.5 \rho u_m^2) \quad (11)$$

The friction factor distribution along the wall is shown in Fig. 5 for the different cases tested. A zoom in the recirculation region is shown in Figure 5b. These values were not available for the traditional  $\kappa$ - $\varepsilon$  model, and they will not be presented here. It can be seen, that the shear stress increases at the convergent region of the duct, reaching a maximum value at the center of the obstruction, with a very sharp drop right after it. The separation point is clearly identified as the position where the shear stress is zero. After this point, the shear stress becomes negative indicating the recirculation region. All models, with the exception of the  $L_\varepsilon=0, C_3=C_1$  case, present an increase of the shear stress after the separation point. However, near the end of the obstruction region, close to the center of the recirculation, where the reverse flow is stronger, a decrease in the shear stress is observed. After which, the shear increases again. When the extra term  $L_\varepsilon$  is zero, the size of the recirculation regions is reduced. As the contribution of the normal in relation to the tangential one is reduced, the size of the recirculation region is further reduced. Once again the influence of the  $L_\varepsilon$  is smaller.

Table 1 presents a comparison of the separation and reattachment points,  $x_s$  and  $x_r$ , predicted by the different models and the results of Rastogi (1984) and Melaane (1992) obtained with the traditional  $\kappa$ - $\varepsilon$  models. The experimental results of Desphane and Giddens

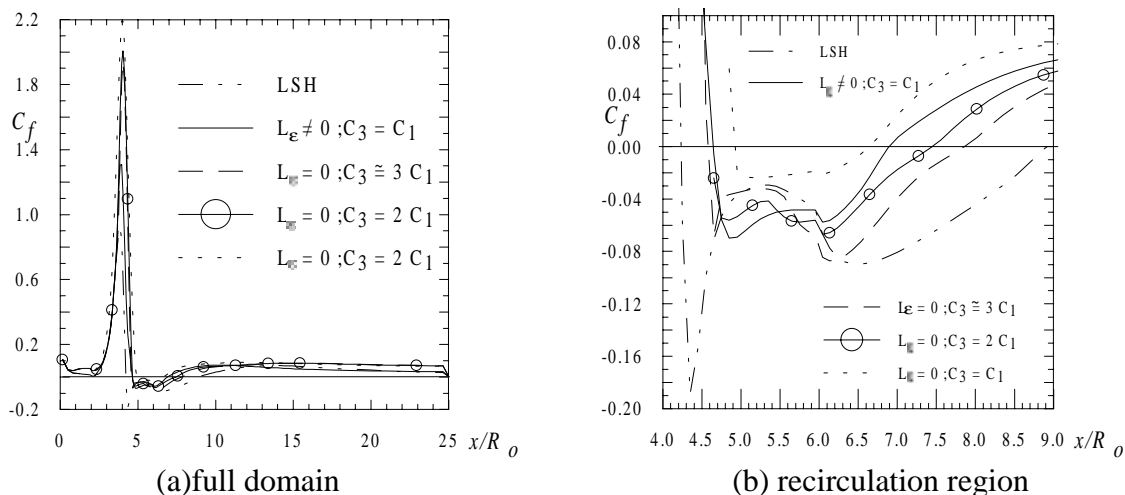


Figure 5 –Friction factor along wall.

(1980) are also shown at the table.

By examining Table 1, it can be seen that the higher order scheme with the traditional  $\kappa$ - $\epsilon$  model (Melaaen, 1992) and the  $L_\epsilon = 0$  case presented the best agreement with experimental data, for both separation and reattachment points. The LSH model underpredicts the separation point and overpredicts the reattachment point. Note that the normal stress is not a factor to determine the separation point, but it significantly affects the flow after separation. The worse result was predicted by Rastogi (1984), however, they are not very different than the ones predicted by the  $C_1=C_3$  with  $L_\epsilon = 0$  and  $C_1=C_3$  with  $L_\epsilon \neq 0$  models.

Table 1 – Separation and reattachment points

Model	$x_s/R_o$	Erro %	$x_r/R_o$	Erro %
Desphande e Giddens, 1980 (experimental)	$\approx 4.4-4.5$		8.0	
Rastogi, 1984	5.2	16	6.4	20
Melaaen, 1992	4.6	3	8.1	1
LSH ; ( $L_\epsilon \neq 0, C_3 \approx 3C_1$ )	4.2	6	8.9	11
$L_\epsilon \neq 0; C_1 = C_3$	4.6	3	6.9	14
$L_\epsilon = 0, C_3 \approx 3C_1$	4.6	3	7.9	1
$L_\epsilon = 0; C_3 = 2C_1$	4.6	3	7.5	6
$L_\epsilon = 0; C_3 = C_1$	4.9	10	6.6	18

### 4.3 Turbulence quantities

The only turbulence quantity available in the literature to allow a comparison with the present results is the turbulent kinetic energy. Figure 6 present its dimensionless distribution,  $\kappa^* = \kappa/u_m^2$ , along the centerline. It can be seen that the agreement of the different numerical and turbulent models with experimental data is not satisfactory. The experimental data show an approximately constant  $\kappa$  up to the section of maximum obstruction. Along the region where pressure is recovered, there is a substantial increase of  $\kappa$ , followed by a strong decrease. The kinetic energy is generated at the obstruction and convected to the rest of the domain. Therefore, the increase on its value is only observed at the centerline further downstream. The section where  $\kappa$  starts to fall corresponds to the section where pressure has reached its downstream level, as can be seen in Fig. 3.

All models presented a sharp increase of  $\kappa$  along the centerline followed by its reduction, however, the section where the maximum occurs, as well as the maximum value are quite different for each case. Note that the maximum  $\kappa$  always corresponds to the point where pressure has reach a constant value. This behavior can also be observed by the experimental data. This means that the numerical models are capable of capturing the relationship of the turbulent quantities with the flow parameters. However, when the turbulence model underestimated  $\kappa$  and  $\epsilon$ , the recirculation region is smaller, the pressure recovery is anticipated.  $C_3=C_1$  cases presented the largest discrepancies with the experimental data, and present two peaks of  $\kappa$ . Melaaen (1992) result also shows two peaks of  $\kappa$ . The first one over estimates  $\kappa$ , while the second one is quite close to the experimental data. The LSH model is not able to reproduce the increase in  $\kappa$  at the obstruction region. It presents a sharp increase of

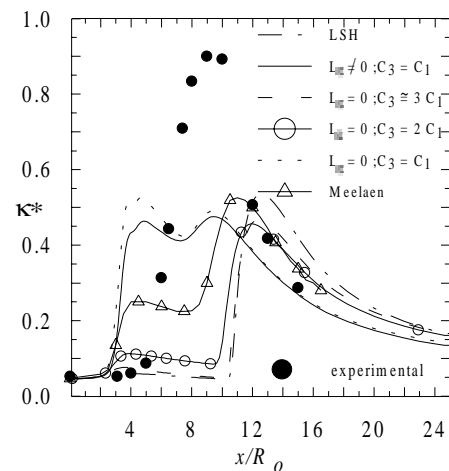


Figure 6 – Centerline turbulent kinetic energy distribution

$\kappa$ , right after the reattachment point. The extra source term  $L_\varepsilon$  did not affect the  $\kappa$  distribution along the centerline. Note that, an increase the normal stress contribution to the production of  $\varepsilon$  reduces the first peak of  $\kappa$ , and anticipates the second peak. The specified value of the LHS model ( $C_3=4.44$ ) seems to be too large, while the  $C_3=1.44$  ( $C_3=C_1$ ) is too small. In fact, the  $C_3=2C_1$  case, which corresponds to  $C_3=2.88$ , also seems to be too large for corrected  $\kappa$  distribution. However, if the  $C_3$  value is increased worse results will be obtained for the pressure, velocity, and friction factor distribution.

To try to understand the results obtained, isocurves of turbulent kinetic energy and dissipation rate are presented at Fig. 7 and Fig. 8, respectively, for the cases tested. In those figures, the low  $\kappa$  and  $\varepsilon$  values are represented by the darker gray and as the gray gets lighter, their values increase. Low  $\kappa$  values can be seen near the entrance for all cases. The turbulent kinetic energy begins increases at the obstruction, as one can see the gray getting lighter. Then it reaches a maximum value at the recirculation region, when a new dark gray appears. The kinetic energy is generated near the wall and then it is convected throughout the domain. The recirculation region predicted by the LSH model is much larger than the other models, and its center of rotation is displaced downstream, as a consequence the maximum turbulent kinetic energy generation also occurs displaced to downstream. The high value generated are then convected, and the increase in  $\kappa$  at the centerline is only seen at section  $x/R_o = 12$ . Examining Fig. 7 and 8, it can be seen that when the normal stress has the same weight as the tangential one in the  $P_\varepsilon$  ( $C_3=C_1$ ), larger  $\kappa$  is obtained in the obstruction region. In fact, larger weight to the normal stress is recommended when there is curvature present in the domain, as is the case. Unfortunately, as the normal stress weight increases, the recirculation region is displaced in the axial direction, and the peak of  $\kappa$  occurs outside the recirculation region, which is not reasonable.

## 5. CONCLUSION

At the present paper, the model developed by Launder and Sharma, and modified by Hanjalic, model LSH, is investigated to predict the flow field in a duct with smooth obstruction. Four variations of the original model were investigated to help understand the influence of each term in the flow field. It was verified that although the velocity and pressure distributions were reasonable predicted by the different models, all of them fail to predict

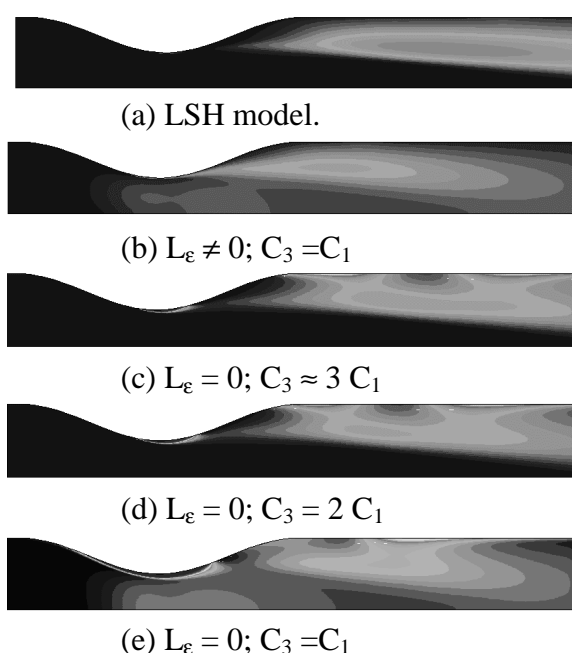


Figure 7 – Turbulent kinetic energy distribution.

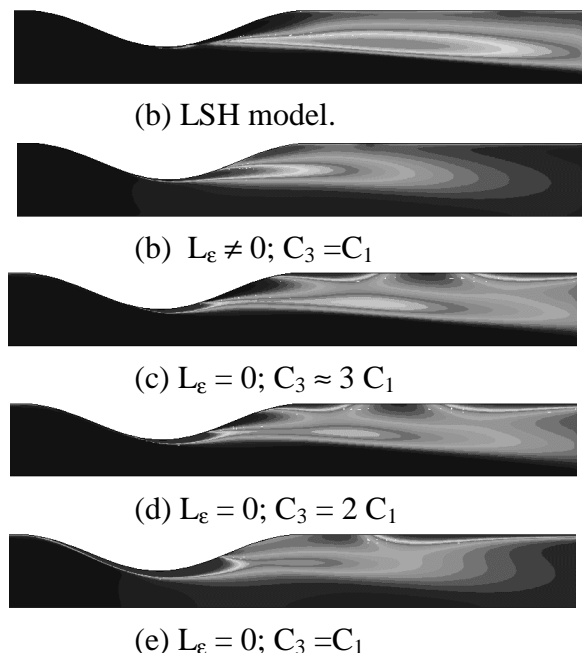


Figure 8 – Dissipation distribution.

correctly the turbulent quantities. The original LSH model presented the best agreement with experimental data. However, the higher order interpolation scheme with the traditional  $\kappa$ - $\varepsilon$  model, also predicted good results. The SSA and NT models are not adequate to predict separation along smooth surfaces, because the low Reynolds models are more expensive and harder to converge and these models presented results equivalent to cheaper and easier to implement traditional  $\kappa$ - $\varepsilon$  models. It seems that a combination of a higher order scheme and the LSH model should be investigated.

## REFERENCES

- Abe K., Kondoh T., Nagano Y., 1994, A New Turbulence Model for Predicting Fluid Flow and Heat Transfer in Separating and Reattaching Flows Part: I Flow Field Calculation, *Int. Journal Heat and Fluid Flow*, vol. 18, n. 3, pp. 266-282.
- Chen S., Lai J., Milthorpe, J., Mudford N., 1998, A New Modified Low-Reynolds Number  $\kappa$ - $\varepsilon$  Model, 29<sup>th</sup> AIAA Fluid Dynamic Conference, AIAA 98-2553.
- Desphande M. D., Giddens D.P., 1980, Turbulence Measurement in a Constricted Tube, *Journal Fluids Mechanics*, vol. 97, pp. 65-89, Part 1.
- Geronimos G., So R. M.C., 1997, Near-Wall Modeling of Plane Turbulent Wall Jets, *J. of Fluids Engineering*, vol. 119, June, pp. 304-313.
- Hanjalic K, Launder B.E., 1980, Sensitizing the Dissipation Equation to Irrotational Strain, *Journal of Fluids Engineering*, vol.102, March, pp. 34-40.
- Jones W.P., Launder B.E., 1972, The Prediction of the Laminarization with a two-equation model of turbulence, *International Journal Heat Mass Transfer*, vol. 15, pp. 301-314.
- Koobus B., 1994, An Implicit Method for Turbulent Boundary Layers Simulation, Programme 6 –Calcul scientifique, modélisation et logiciel numérique, Unité de Recherche INRIA Sophia - Antipolis.
- Melaaen M. C., 1992, Analysis of Fluid Flow in Constricted Tubes and Ducts Using Body-Fitted Non-Staggered Grids, *International Journal for Numerical Methods in Fluids*, vol. 15, pp. 895-923.
- Patankar S. V., 1980, *Numerical Heat Transfer and Fluid Flow*, Hemisphere, New York.
- Patel V., Rodi W., Scheuerer G., 1985, Turbulence Models for Near-Wall and Low-Reynolds Number Flows: A Review, *AIAA Journal*, vol. 23, n. 9, pp. 1308-1319.
- Pires, L. F. G. and Nieckele, A. O., 1994, Numerical Method For The Solution Of Flows Using Contravariant Components In Non-Orthogonal Coordinates, *Proc. V Brazilian Meeting on Thermal Sciences*, pp. 343-346 (in Portuguese).
- Rastogi A. K., 1984, Hydrodynamics in Tubes Perturbed by Curvilinear Obstructions, *Journal of Fluids Engineering*, vol. 106, September, pp. 262-269.
- Sarkar A., So R.M., 1997, A Critical Evaluation of Near Wall Two-Equation Models Against Direct Numerical Simulation Data, *Int. J. Heat and Fluid Flow*, vol. 18, pp. 197-208.
- Settari A., Aziz K., 1973, A Generalization of the Additive Corrections Methods for the Iterative Solution of Matrix Equations, *SIAM, J. Num Analysis*, vol. 10, pp. 506-521.
- Shima K., Candler G., 1998, Convergence Improvement of Two-Equation Turbulence Models Calculations, 29<sup>th</sup> AIAA Fluid Dynamics Conference, AIAA 98-2649.
- Van Doormaal, J. P. Raithby, G. D., 1984 Enhancements of the Simple Methods for Prediction Incompressible Fluid Flow, *Num. Heat Transfer*, vol. 7, pp. 147-163.
- Zevallos G.A. Nieckele A., 1999, Performance of K-E Low-Reynolds Models To Predict Flow Through Curvilinear Obstruction", *Congresso Brasileiro de Engenharia Mecânica, COBEM99, CD-ROM, Sessão Técnica: Fluid Mechanics - código AACGHJ*.
- Zijlema M., Segal A., Wessling P., 1995, Finite Volume computation of 2D incompressible turbulent flows in general coordinates on staggered grids, <http://www.dutita0.twi.tudelft.nl/isnas/report94-24/isrep2.html>.